journal

J. Am. Ceram. Soc., 94 [4] 1281–1288 (2011)
DOI: 10.1111/j.1551-2916.2010.04228.x

Influence of MgO, SrO, and ZnO Dopants on Electro-Thermal Polarization Behavior and In Vitro Biological Properties of Hydroxyapatite Ceramics

Subhadip Bodhak, Susmita Bose, and Amit Bandyopadhyay†

W. M. Keck Biomedical Materials Research Laboratory, School of Mechanical and Materials Engineering, Washington State University, Pullman, Washington 99164

The objective of this work was to investigate the influence of trace element (Mg^{2+}, Zn^{2+}, and Sr^{2+}) doping on polarization behavior of sintered hydroxyapatite [HAp, $Ca_{10}(PO_4)_6(OH)_2$] pertinent to biomedical applications. For this purpose, commercially procured phase pure HAp powder was doped with MgO, SrO, and ZnO dopants in different single, binary, and ternary compositions. All samples were sintered at 1200°C for 2 h and subsequently electro-thermally polarized via application of an external dc field (2.0 kV/cm) at 400°C. Combined addition of 1 wt% MgO/1 wt% SrO in HAp was found to be the most beneficial in enhancing the polarizability (stored charge ~4.19 μC/cm^2) of pure HAp (stored charge ~2.23 μC/cm^2) by inhibiting high-temperature HAp phase decomposition. Furthermore, *in vitro* bone cell–material interaction has been studied for polarized binary doped (1 wt% MgO+1 wt% SrO in HAp) HAp samples by culturing with human fetal osteoblast cells for a maximum of 7 days to establish the significance of dopants on polarized HAp for bone graft applications. Scanning electron microscope images of cell morphology revealed that favorable surface properties and dopants chemistry led to good cellular adherence and extracellular matrix formation on negatively charged surfaces of binary doped HAp samples in comparison with undoped HAp surfaces. MTT assay results at 7 days showed the highest cell proliferation on negatively charged surfaces of binary doped HAp samples.

I. Introduction

HYDROXYAPATITE [HAp, $Ca_{10}(PO_4)_6(OH)_2$] has been recognized as one of the most widely researched bioceramics due to its excellent biocompatibility; ability to promote cellular functions, and protein expressions in both *in vitro* and *in vivo* conditions. It is commonly used as a filler to replace amputated bone or as a coating on load-bearing orthopedic implants to promote bone ingrowth.[1,2] However, one of the major drawbacks of synthetic HAp is its inferior osteogenic capacity and poor mechanical strength compared with the living bone tissue, and this has been attributed to the subtle but significant chemical difference found in the structure. Earlier studies show that natural bone contains different trace elements such as Mg^{2+}, Sr^{2+}, Zn^{2+}, F^-, and CO_3^{2-}, which play an important role in biological and mechanical performances of bone and this subtle but significant chemical difference found in the natural bone structure has been attributed to the one of the important reason of lower osteogenic capacity as well mechanical properties of synthetic HAp.[3–5] In recent years, several studies have been reported on the synthesis of metal ion substituted HAp and shown to improve its structural stability and cellular biocompatibility properties.[6–11]

Recently, significant research has been invested on improving the osteoductivity of HAp using electro-thermal polarization treatment as a surface modification technique with a surface charge between 0.08 and 1.2 mC/cm^2 depending on the applied electric field strength and polarization temperature.[12–25] The original concept of polarized HAp to be used as bone graft material was first introduced by Yamashita *et al.*[17] during the late 1990s. It was shown that the electrostatic charges present on poled HAp surfaces can significantly accelerate or decelerate bone-like apatite deposition in simulated body fluid depending on the surface charge amount and it's polarity. Following this, a number of *in vitro* and *in vivo* studies have investigated the effect of electrical charges and polarization conditions on the biological response to polarized HAp toward orthopedic and reconstructive implant applications.[18–25] In our previous research, we have shown that bulk sintered HAp wettability and surface energy can be tailored by inducing a surface charge through electro-thermal polarization treatment without introducing any volumetric effects in the material.[21] It has been demonstrated that the combined influence of surface charge density, surface energy, and surface wettability enabled early-stage mineralization as well as significantly improved the bone cell adhesion and growth on electro-thermally polarized HAp compacts depending on the polarity of the surface charge.[21] Similar observation has also been made and showed that water contact angle values on neutral surface of HAp can be significantly decreased from 60° to 25° on positively charged HAp surface under optimum poling condition.[22] Furthermore, the application of polarization in HAp coating application has also been successfully implemented.[24] Our group further strengthens the polarized HAp research by reporting experimental observations on early-stage cell anchorage as well as differentiation by vinculin and alkaline phosphatase protein expression for a range of incubation periods to unveil the bone cell–material interactions.[25]

However, till date, no experimental investigation has been carried out to understand electro-thermal polarization treatment and/or *in vitro* bone cell–material interactions of electrically polarized HAp ceramics doped with different trace elements, which can show an additional advantage of matching bone chemistry along with the original benefits of electrical polarization treatment. For this purpose, based on literature review[6–11] and our own previous research,[5,26–29] we have identified a selected group of trace elements such as Mg^{2+}, Sr^{2+}, and Zn^{2+} as potential dopants. Previous investigation revealed that the presence of Mg^{2+} can influence the mineral metabolism and promote catalytic reactions during the bone remodeling process.[30] Mg-doped HAp has also been reported to improve the fracture strength as compared with pure HAp. Earlier *in vitro* and *in vivo* studies have also indicated that strontium increases osteoclast apoptosis and enhances preosteoblastic cell proliferation and collagen synthesis.[31,32] On the other hand, Zn has a direct proliferative effect on the osteoblastic cells and a potent and selective inhibitory effect on osteoclastic bone resorption activities.[33]

J. Ferreira—contributing editor

Manuscript No. 27976. Received May 5 2010; approved October 4 2010.

This work was financially supported by the Office of Naval Research under the grant no. N00014-01-05-0583, and the National Institutes of Health under the grant no. NIH-R01-EB-007351.

†Author to whom correspondence should be addressed. e-mail: amitband@wsu.edu

Therefore, it is important to incorporate these trace elements into synthetic HAp to improve its mechanical and biological performance. Furthermore, it has been observed that the HAp lattice easily incorporates these metallic dopants in the apatite structure, inducing modifications in the lattice parameters and the thermal stability. Therefore, we hypothesize that the poling behavior of HAp can be optimized by doping these trace elements that have a significant influence on the structural stability of HAp and further the combined influence of dopants and polarization may assist in designing bone graft materials that can permit rapid cell growth while providing the initial biomechanical support required for the restoration of ambulatory function. In the present report, we have investigated how the various dopants in different single, binary, and ternary compositions influence the polarization behavior of HAp and evaluated the combined influence of dopants and surface charge on bone cell interactions on polarized doped HAp surfaces in *in vitro* condition.

II. Materials and Methods

(1) Sample Preparation

Commercially procured phase pure HAp (Berkley Advanced Biomaterials Inc., Berkeley, CA) was doped using 1.0 wt% MgO, 1.0 wt% SrO, and 0.25 wt% ZnO as dopants (99.9% purity) in different single, binary (1.0 wt% MgO+1.0 wt% SrO), and ternary (1.0 wt% MgO+1.0 wt% SrO+0.25 wt% ZnO) compositions. The amount of dopants was selected based on our previous research and the reported literature. Previous investigation showed that the selected dopants improved the biological and mechanical properties of calcium phosphate ceramics when used in trace amount.[5,9,27,29] Specific amounts of dopants were added into HAp and the mixtures were wet ball milled in ethanol media for 24 h at 70 rpm. After ball milling, powders were then placed in an oven at 80°C for 72 h for drying. Dried powders were then pressed using a uniaxial press to form disks [diameter (Φ) ~12 mm and height (h) ~1 mm] and sintered in air at 1200°C for 2 h in a conventional muffle furnace.

(2) Phase Analysis and Density Measurement

Phase analyses of ground powders prepared from sintered samples were performed using an X-ray diffractometer (Philips PW 3040/00 X'pert MPD, Eindhoven, the Netherlands) using Cu Kα radiation at 30 kV and 35 mA with a Ni filter. The bulk densities of the sintered doped and undoped HAp were measured by the Archimedian's method.[34] The amount (the wt% fraction) of different phases (i.e., HAp, β-tricalcium phosphate (TCP), tetra tricalcium phosphate (TTCP), CaO) present in the sintered undoped and doped HAp samples was quantitatively determined by using the ratio of the relative intensities of the most prominent or highest diffracted XRD peaks of the respective phases by the the following equation[35]:

$$W_{\text{Calculated Phase}} = \frac{I_{\text{Calculated Phase}}}{I_{\text{Calculated Phase}} + \sum I_{\text{Other Phase}}} \quad (1)$$

where $W_{\text{Calculated Phase}}$ is the wt% of the calculated phase, $I_{\text{Calculated Phase}}$ is the relative intensity or the peak height of the most prominent XRD peak of the corresponding phase, and $I_{\text{Other Phase}}$ is the relative intensity of the most prominent XRD peaks of other phases.

To compare densification of different doped and undoped sintered samples, relative densities (% theoretical) were calculated from the theoretical densities of the starting powders. The theoretical densities of the different sintered samples were calculated using rule of mixture based on XRD phase analysis results using the the following equation[34]:

$$\text{T.D.} = \frac{1}{\sum \frac{W_x}{D_x}} \quad (2)$$

where T.D. is the calculated theoretical density of the sintered sample, W_x is the wt% of the phase x present in the sample, and D_x is the theoretical or powder density of the corresponding phase x. For sintered sample theoretical density calculation, the theoretical densities of HAp, β-TCP, TTCP, and CaO were taken as 3.16, 3.07, 3.06, and 3.35 g/cm^3, respectively.

(3) Electro-Thermal Polarization and Thermally Stimulated Depolarization Current (TSDC) Measurement

Electro-thermal polarization was carried out on the sintered and polished undoped and doped HAp samples in air, using platinum electrodes with a Keithley 6487 picoammeter (Keithley Instruments Inc., Cleveland, OH) and a ceramic strip heater (OMEGA Engineering Inc., Stamford, CT). During polarization, the samples were slowly heated from the room temperature to the polarization temperature (T_p) with a controlled heating rate of 5°C/min and soaked at T_p for 1 h before applying a dc voltage. A dc electrical field (E_p) of 2.0 kV/cm was applied for 1 h at T_p and maintained until the sample cooled to the room temperature. The polarity of the induced surface charges depends on the applied external dc field polarity, while the magnitude of the stored charge depends on the polarization temperature. In order to estimate the stored static charge due to the polarization operation, TSDC technique was used.[36] Polarized HAp samples were heated at a rate of 5°C/min up to 550°C and the thermally stimulated release depolarization current was measured using a Keithley 6487 picoammeter. The stored electrical charge was calculated from the TSDC spectra using the the following equation.[21]

$$Q_p = \frac{1}{\beta} \int J(T) \mathrm{d}T \quad (3)$$

where Q_p denotes the stored charge density β and $J(T)$ are the heating rate and the current density, respectively.

(4) In Vitro Bone Cell–Material Interactions

In vitro cytotoxicity behavior of poled, and unpoled undoped and doped HAp samples was evaluated to investigate the influence of the dopants and polarization on osteoblast cells. For this purpose, based on the TSDC study results, binary-doped HAp samples were selected and used in bone cell–material interaction study because the combined addition of 1 wt% MgO/1 wt% SrO in HAp was found to be the most beneficial in enhancing the polarizability of HAp. For comparison, undoped HAp samples were used as control. *In vitro* cytotoxicity behavior of all negatively charged, positively charged, and unpoled binary doped as well as undoped HAp samples was evaluated for 3 and 7 days of incubation using human fetal osteoblast cells (hFOB). The cells used were derived from an immortalized, osteoblastic cell line, established from human fetal bone tissue. All samples were sterilized by autoclaving at 121°C for 20 min before cell culture experiment. Following this, cells were seeded onto HAp samples polarized at 400°C, placed into the wells of a 24-well plate with either the negative-charged ("N" poled) or positive-charged ("P" poled) surfaces facing upward. Nonpolarized undoped as well as doped HAp samples were used as controls in our investigation. Initial cell density was 1.0×10^4 cells/wall. One milliliters of DMEM media enriched with 10% fetal bovine serum was added to each well. Cultures were maintained at 34°C under an atmosphere of 5% CO_2 and 95% air in an incubator. The culture media were changed every alternate day during the duration of the experiment. From here on, the negatively polarized surface will be termed as "N" poled surface and positively polarized surface as "P" poled surface.

(A) Cell Morphology: Cells morphology was assessed by scanning electron microscope (SEM) observation after 7 days of culture period. Cultured samples for SEM observation were rinsed with 0.1*M* phosphate-buffered saline (PBS) and fixed with 2% paraformaldehyde/2% glutaraldehyde in 0.1*M* cacodylate buffer overnight at 4°C. Following this, post fixation for

each sample was made with 2% osmium tetroxide (OsO_4) for 2 h at room temperature. Fixed samples were then dehydrated in an ethanol series 30%, 50%, 70%, 95%, and 100% three times, followed by a hexamethyldisilane drying procedure. Dried samples were then mounted on aluminum stubs, gold coated, and observed under a field-emission SEM (FEI Inc., Hillsboro, OR).

(B) Cell Proliferation Using MTT Assay: The MTT (3-(4,5-dimethylthiazol-2-yl)-2,5-diphenyl tetrazolium bromide) assay (Sigma Inc., St. Louis, MO) was performed for 3 and 7 days of incubation to determine hFOB cell proliferation on polarized as well as nonpolarized doped and undoped HAp surfaces. Triplicate samples per group were evaluated and three data points were measured from each sample. The MTT (Sigma) solution of 5 mg/mL was prepared by dissolving MTT in PBS, and was filter-sterilized using a filter paper of 0.2 μm pore. The MTT was diluted (100 μL × 900 μL) in DMEM/F12 medium. One milliliter of diluted MTT solution was then added to each sample in 24-well plates. After 2 h of incubation, 1 mL of solubilization solution made up of 10% Triton X-100, 0.1 N HCl, and isopropanol was added to dissolve the formazan crystals. One hundred microliters of the resulting supernatant was transferred into a 96-well plate, and read by a plate reader at 570 nm.

(5) Statistical Analysis

Triplicate samples were used in all the experiments to ensure reproducibility. Data for densification and MTT assay are presented as mean ± standard deviation. Statistical analysis was performed on relative densities of different sintered samples and MTT assay results using Student's *t*-test and a *P*-value <0.05 was considered significant.

III. Results and Discussion

(1) Phase Evaluation and Densification

Figure 1 presents the XRD spectra acquired from commercially procured HAp powder, as well as sintered undoped and doped HAp samples. The XRD pattern from commercial powder shows only characteristic peaks of HAp phase, which match well with the JCPDS card (09-0432) as shown in Fig. 1(a). However, XRD pattern from sintered HAp reveals that both undoped and doped HAp samples with different concentrations of dopants exhibit characteristic HAp [$Ca_{10}(PO_4)_6(OH)_2$] peaks along with the varying concentration of β-TCP phase (JCPDS No. 09-0169) and the occasional presence of the weak additional

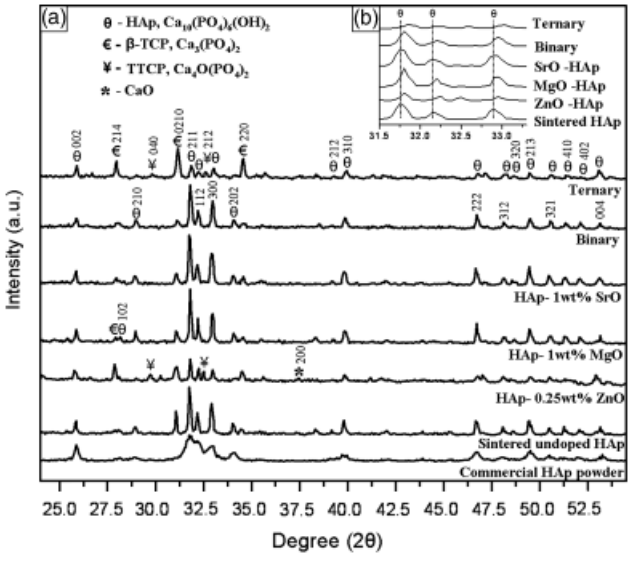

Fig. 1. (a) Comparison of XRD patterns of commercial HAp powder, sintered undoped HAp and doped HAp samples, (b) XRD patterns for sintered doped and undoped HAp samples illustrating the shift in peaks due to incorporation of dopants.

peaks correspond to TTCP (JCPDS No. 25-1137) and CaO (JCPDS No. 04-0777). It can be recalled earlier that research reports have proved that the sintering of HAp can lead to the dehydroxylation (removal of OH^-) and partial thermal decomposition of HAp into varying amount of TCP, CaO, and/or TTCP phases depending on several factors such as sintering temperature, heating atmosphere, starting powder physical properties etc.[37–39] In Fig. 1(a), XRD pattern from the undoped HAp reveals the dominant presence of β-TCP phase (JCPDS # 09-0169) along with characteristic peaks of HAp phase. The decomposition of HAp into β-TCP occurs at a temperature $>900^\circ C$ according to the the following equation:

$$Ca_{10}(PO_4)_6(OH)_2 \rightarrow 3Ca_3(PO_4)_2 + CaO + H_2O \quad (4)$$

However, it can be seen that the presence of Mg and Sr dopants considerably improves the thermal stability of HAp crystal structure compared with undoped HAp. Weak peaks of β-TCP for SrO-doped HAp clearly indicate less decomposition of HAp phase during the sintering process. The influence of MgO dopant is more pronounced in stabilizing the HAp phase and MgO dopant in both single and binary dopant composition has been found to inhibit the decomposition of HAp. Table I presents the amount of different phases as obtained in different sintered doped and undoped HAp samples. The quantitative calculation of different phases from XRD results has evidently showed that the amount of HAp (wt%) is higher for MgO-doped HAp (91.5 wt% HAp, 9 wt% β-TCP), SrO-doped HAp (84 wt% HAp, 16 wt% β-TCP), and binary-doped HAp samples (~88 wt% HAp, 12 wt% β-TCP) as compared with pure HAp (HAp phase ~67 wt%, β-TCP phase ~33 wt%).

However, the addition of ZnO has been found to have a minimal influence on HAp phase stabilization. For both ZnO-doped single and ternary HAp samples, the presence of Zn is observed to destabilize the HAp phase as indicated by the strong peaks of β-TCP. The quantitative calculation also confirms that Zn leads to destabilize the HAp phase and considerably lower amount of HAp is measured for ZnO-doped HAp samples (HAp phase ~49 wt%, β-TCP phase ~33 wt%) as compared with MgO- or SrO-doped and undoped HAp samples. In particular, for ternary doped HAp sample the incorporation of ZnO has been observed to stabilize the β-TCP phase (HAp phase ~20 wt%, β-TCP phase ~67 wt%). This observation is in good agreement with earlier reported work.[40–42] Bigi and colleagues showed that zinc preferentially enters into the β-TCP structure and stabilized the β-TCP phase. In addition, the presence of TTCP phase along with a weak peak of CaO can also be noticed for Zn-doped samples because of the increasing thermal decomposition of HAp phase. The formation of TTCP phase can be explained by the following possible reaction as given in the following equation:

$$Ca_{10}(PO_4)_6(OH)_2 \rightarrow 2Ca_3(PO_4)_2 + Ca_4P_2O_9 + H_2O \quad (5)$$

Figure 2 shows the densification results (as % theoretical density) for the sintered doped and undoped HAp samples. Based on the XRD analysis, the theoretical densities of each composition has been calculated and presented in Table I. In Fig. 2, the relative densities of different samples are presented as determined from the measured bulk densities and calculated theoretical densities of different samples. Undoped HAp shows a relatively low density (93.93% ± 1.92%) after sintering at 1200°C for 2 h compared with the single doped or binary doped HAp samples. This result is expected because the dissociation of HAp into a less dense β-TCP causes the lattice volume expansion during HAp to β-TCP phase transition, which lowers the density of undoped HAp samples. However, the density of HAp can be significantly improved after addition of MgO as dopants as confirmed by statistical analysis ($^*P>0.05$). A maximum density of 98.83% ± 1.11% can be achieved by adding 1 wt% MgO into HAp. It can be suggested that during sintering the bivalent smaller ionic radius Mg^{2+} ion (0.66 Å) substitutes a

Table I. Calculation of Different Phases and the Theoretical Densities (g/cm^3) Based on XRD Quantification for Various Doped and Undoped HAp Samples Sintered at 1200°C or 2 h

Sample	Presence of phases (wt%)				Measured bulk density (g/cm^3)	Calculated theoretical density (g/cm^3)	Relative density (% theoretical density) (%)
	HAp	β-TCP	TTCP	CaO			
Undoped HAp	66.67	33.33			2.94±0.06	3.13	93.93±1.92
HAp–1 wt% SrO	84.25	15.75			2.94±0.03	3.14	93.63±0.84
HAp–1 wt% ZnO	49.09	32.90	12.27	5.74	2.95±0.03	3.13	94.14±0.8
HAp–1 wt% MgO	91.57	8.53			3.10±0.04	3.14	98.83±1.11
Binary doped HAp	88.06	11.94			3.08±0.03	3.14	98.19±0.97
Ternary doped HAp	19.88	66.27	7.83	6.02	2.90±0.03	3.10	93.44±0.81

HAp, hydroxyapatite; TTCP, tetra tricalcium phosphate; TCP, tricalcium phosphate.

higher ionic radius Ca^{2+} ion (0.99 Å) in the HAp crystal lattice structure. This leads to shrinking of the unit cell of HAp lattice and increases the density of MgO-doped HAp samples. This conclusion is supported by the XRD result (Fig. 1(b)), which indicates a peak shift toward higher angle side for MgO-doped HAp samples in both single and binary composition. However, although Zn^{2+} has lower ionic radius (0.74 Å) than Ca^{2+} ion (0.99 Å), ZnO doping shows no improvement in density in comparison with undoped HAp. Both ZnO-doped single and ternary HAp samples exhibit low theoretical densities of 94.14%±0.8% and 93.44%±0.81%, respectively, which are almost similar to the density of undoped HAp. It is believed that in spite of having lower ionic radius than Ca^{2+} ions, unlike Mg for MgO-doped samples, Zn doping inhibits HAp stability, and preferentially stabilizes the β-TCP, which consequently leads to decrease the density of ZnO-doped HAp samples due to the dominant presence of less dense β-TCP and other phases (TTCP and CaO).[40–43] In the case of Sr^{2+}-doped HAp, which has higher ionic radius (1.13 Å) than Ca^{2+} ion leads to expansion of HAp crystal lattice by substituting a lower ionic radius Ca^{2+} ion (0.99 Å) and reduces the density of HAp (93.63%±0.84%) despite the improved thermal stability of HAp and the lower concentration of β-TCP phase as compared with undoped and ZnO-doped HAp samples. The statistical analysis on relative densities data of different sintered samples reveals that the differences in densities between pure/undoped sintered HAp and three different doped sintered HAp samples (ZnO–HAp-, SrO–HAp-, and ternary doped HAp) are not statistically significant ($^{**}P>0.05$). However, binary doped HAp sample shows significant improvement in the density (98.19%±0.97%) in comparison with undoped HAp as confirmed by the Student *t*-test ($^{*}P<0.05$). It is believed that the average size of substituted Sr^{2+} and Mg^{2+} ions (1.13 Å+0.66 Å)/2 = 0.90 Å being lower than the substituted Ca^{2+} ion size which leads to decrease in the unit cell parameters of HAp structure and hence shift in the peak to higher 2θ value is observed (Fig. 1(b)).[11] Interestingly, statistical analysis indicates that the relative density difference between MgO–HAp and binary doped HAp samples is not significant ($P>0.05$).

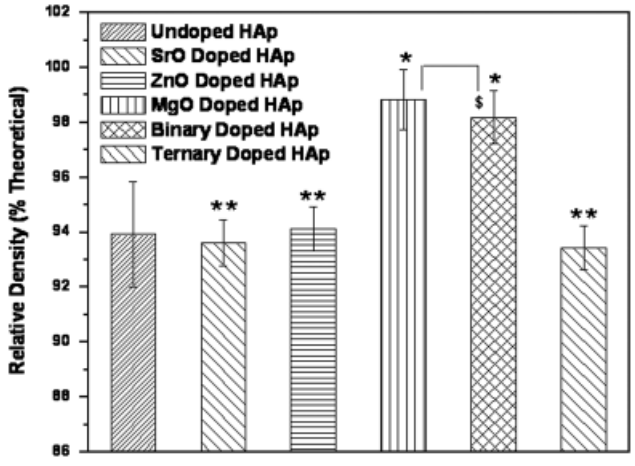

Fig. 2. Relative density variation for different sintered undoped HAp and doped HAp samples. Statistical analysis confirms that the differences in relative densities between undoped HAp and SrO–HAp, ZnO–HAp, ternary HAp are not significant ($^{**}P>0.05$) whereas the differences in relative densities between undoped HAp and MgO–HAp as well as undoped HAp and binary doped HAp samples are significant ($^{*}P<0.05$). Statistical analysis also indicates that the relative density difference between MgO–HAp and binary doped HAp samples is not significant ($^{\$}P>0.05$).

(2) Polarizability and Stored Charge Characterization

To understand the influence of different dopants on the polarizability and charge storage ability of sintered HAp ceramics, TSDC technique was used to confirm the success of the polarization treatment. Figure 3 shows the characteristic TSDC thermograms measured for different doped and undoped polarized HAp samples. The calculated stored charge (Q_p) values are presented in Table II. The value of Q_p for the polarized undoped HAp compact has been estimated as 2.23 μC/cm^2. However, a considerable difference in the polarizability behavior can be observed for doped HAp samples from the TSDC thermographs as shown in Fig. 3 and the calculated stored charge results as presented in Table II. Interestingly, the stored charge density of doped HAp is gradually increased from 2.37 μC/cm^2 with the addition of SrO into HAp. Furthermore, significant enhancement in polarizability of HAp can be observed with the incorporation of MgO. MgO in single dopant condition in commercial HAp exhibits considerably higher current density of 3.58 nA/cm^2 and stored charge density of 3.86 μC/cm^2, where

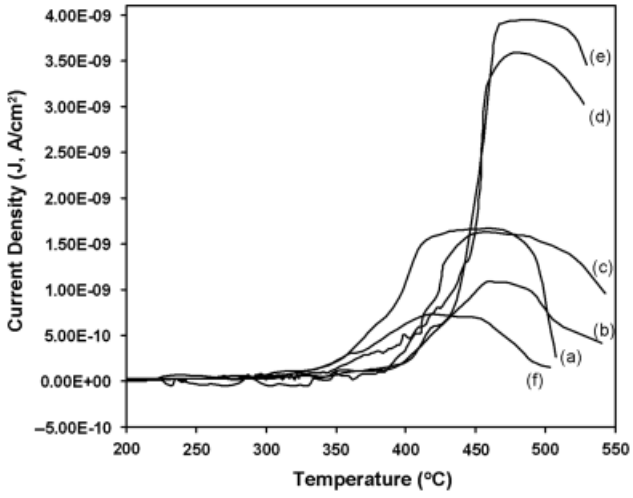

Fig. 3. Thermally stimulated depolarization current curves for (a) undoped HAp, (b) HAp–0.25 wt% ZnO, (c) HAp–1.0 wt% SrO, (d) HAp–1.0 wt% MgO, (e) HAp–1.0 wt% MgO–1.0 wt% SrO, (f) ternary doped HAp samples. Polarization condition: All samples were polarized at 400°C under a dc electric field of 2.0 kV/cm for 1 h.

Table II. Estimated Maximum Current Densities and Corresponding Temperatures Along with the Calculated Stored Charge Values Obtained from Depolarization of Different Doped and Undoped Sintered HAp Samples

Sample	Maximum current density (nA/cm^2)	Temperature at maximum current density (°C)	Stored charge density (Q_p) ($\mu C/cm^2$)
Undoped HAp	1.66	465.4	2.23
0.25 wt% ZnO-doped HAp	1.09	457.4	1.41
1 wt% SrO-doped HAp	1.61	448.7	2.37
1 wt% MgO-doped HAp	3.58	484.3	3.86
1 wt% MgO–1 wt% SrO-doped HAp	3.95	490.9	4.19
1 wt% MgO–1 wt% SrO–0.25 wt% ZnO-doped HAp	0.70	437.4	0.92

Literature results

Sample	Polarization condition	Sintering atmosphere	Maximum current density (nA/cm^2)	Stored charge (Q_p) ($\mu C/cm^2$)	Reference
Sintered HAp	$T_p = 400°C$, $E_p = 2.0$ kV/cm, $t_p = 1.0$ h	Air	4.37	4.28	Bodhak *et al.*[21]
HAp coating on Ti	$T_p = 400°C$, $E_p = 2.0$ kV/cm, $t_p = 1.0$ h	Air	1.19	1.69	Bodhak *et al.*[25]
Sintered HAp	$T_p = 300°C$, $E_p = 1.0$ kV/cm, $t_p = 1.0$ h	Water vapor	3.06	4.20	Nakamura *et al.*[14]
Sintered HAp	$T_p = 400°C$, $E_p = 5.0$ kV/cm, $t_p = 1.0$ h	Water vapor	—	18.00	Ueshina *et al.*[15]
Sintered HAp	$T_p = 600°C$, $E_p = 5.0$ kV/cm, $t_p = 1.0$ h	Water vapor	—	1200	Ueshina *et al.*[15]
HAp (avg. grain size 1.9 μm)	$T_p = 400°C$, $E_p = 5.0$ kV/cm, $t_p = 1.0$ h	Water vapor	—	8.4	Tanaka *et al.*[16]
HAp (avg. grain size 11 μm)	$T_p = 400°C$, $E_p = 5.0$ kV/cm, $t_p = 1.0$ h	Water vapor	—	60	Tanaka *et al.*[16]
Commercially procured porous HAp (75% porosity)	$T_p = 400°C$, $E_p = 2.0$ kV/cm, $t_p = 1.0$ h	—	—	13.0	Iwasaki *et al.*[20]
Dense HA ceramics with drilled hole	$T_p = 400°C$, $E_p = 1.3$ kV/cm, $t_p = 1.0$ h	—	—	2.6	Iwasaki *et al.*[20]
Sintered HAp	$T_p = 600°C$, $E_p = 3.0$ kV/cm, $t_p = 1.0$ h	Water vapor	26.0	—	Kumar *et al.*[23]
Sintered HAp	$T_p = 600°C$, $E_p = 3.0$ kV/cm, $t_p = 1.0$ h	Air	4.0	—	Kumar *et al.*[23]

For comparison, depolarization behaviors of other polarized sintered HAp compacts as reported in the literatures, are also mentioned. Polarization condition: All samples in our present research were sintered in air and electro-thermally polarized at 400°C under an electric field of 2.0 kV/cm for 1 h. HAp, Hydroxyapatite.

as combined addition of 1.0 wt% MgO/1.0 wt% SrO has been found to be the most beneficial in enhancing the polarizability of sintered HAp prepared from commercial powder. A maximum current density and the stored charge density can be achieved as 3.95 nA/cm^2 and 4.19 $\mu C/cm^2$ respectively for the combined addition of MgO and SrO dopants in HAp. This observation is consistent with the XRD results and relative density data, which clearly indicate a significant enhancement in HAp phase thermal stability with the addition of MgO and SrO and improvement of density in presence of MgO. On the contrary, the addition of ZnO can be seen to decrease the polarizabilty of both 0.25 wt% ZnO-doped HAp and ternary doped HAp samples by impairing the density as well as the HAp phase thermal stability and consequently leads to a low stored charge density of 1.41 and 0.92 $\mu C/cm^2$, respectively. Therefore, the TSDC results and the calculated depolarization data as given in Table II clearly indicate that the polarizability and/or charge storage ability of different samples considerably vary with dopant chemistry. Now further to justify the observed influence of different dopants on polarizability behavior of HAp it is important to understand the basic electro-thermal poling mechanism of HAp. Here, it can be recalled that the polarization of HAp has been attributed to the ionic conduction mechanism, where protons (H^+) from the hydroxyl group (OH^-) are considered as the mobile charge carriers that migrate along the columnar (OH^-) channels of hexagonal unit cell of HAp at low temperature (Poling temperature up to 400°C) where as at higher temperature (> 500°C) partial diffusion of O^{2-} can occur along with the proton (H^+) migration.[14,15] Therefore, phase purity is very important for HAp's polarization and charge storage ability of sintered HAp because β-TCP cannot be polarized due to the absence of any hydroxyl group in its crystal lattice. It is reported that a decrease HAp phase content reduces the charge carrier density, which results in lowering the polarizability of HAp samples.[12,13] Furthermore, the degree of densification or the porosity also has a strong influence on polarization level along with the effect of HAp phase purity. With increasing the pore fraction or lowering the density, polarizability is expected to be reduced because the air present inside the pores restricts polarization.

In our present study, we found that polarizability of HAp significantly varies with the dopant chemistry since both the two factors i.e., fraction of the HAp phase (wt%) as well as density or porosity level changes considerably with the presence of dopants, which in turn influences the polarizability and/or charge storage ability of sintered HAp. It has been assumed that the differences in polarizability of undoped HAp, ZnO–HAp, SrO—HAp, and ternary doped HAp are solely due to the difference in the degree of HAp phase stability or fraction of the HAp phase (wt%) because all these samples exhibit similar level of densification. For example, the incorporation of ZnO has been found to lower HAp polarizability for both ZnO-doped and ternary doped sintered HAp samples. This can be attributed to increase the thermal instability of the HAp (ZnO-HAp ~49 wt%, ternary HAp ~20 wt%), which partially dissociate into β-TCP due to dehydroxylation (removal of OH^-) of HAp crystal structure in the presence of ZnO. In contrast, SrO-doped HAp exhibited higher polarizability and better charge storage ability than undoped HAp due to the higher content of HAp phase (HAp ~84 wt%) even if both of them possess similar porosity level. The combined influence of enhanced density as well as higher content of HAp phase can be realized when the polarization behavior of MgO-doped HAp samples to that of

undoped HAp are compared. Higher density or reduced porosity level of MgO- and binary-doped HAp samples as compared with undoped HAp leads to an increase in polarizability in addition to the positive contribution from the higher content of HAp phase present in these samples. Both MgO-doped and binary doped HAp samples exhibit strong and high depolarization current release peaks indicating improved polarizability and comparable charge storage ability. However, when compared between SrO-doped HAp and MgO- or MgO/SrO-doped sample polarizability, it can be observed that for SrO-doped HAp samples, the polarizability and/or charge storage ability are considerably lower due to poor densification.

Our measured surface charge density numbers for different doped and undoped HAp sample are consistent with the literature results as given in Table I. In our previous work, we estimated a stored charge density of 4.28 $\mu C/cm^2$ for sintered pure HAp sample prepared from our laboratory synthesized sol–gel-derived HAp powder.[21] It is believed that synthesis of sol–gel-derived HAp powder at the high pH favors HAp crystal structure stabilization by inhibiting its phase decomposition at higher sintering temperature and therefore can store higher charge than sintered HAp compacts prepared from commercially procured powder.[44] Moreover, it has been observed that the HAp compacts sintered in water vapor exhibited better polarizability due to the reduced dehydration reaction during sintering and better sinterability of HAp compacts.[12–15,37] Nakamura and colleagues reported that a water vapor sintered HAp compact with near theoretical density can store a surface charge of as high as 18 $\mu C/cm^2$ at 400°C.[14,15] In another report, polarized HAp sintered in both air and water vapor exhibited a depolarization a peak current density of 4 and 26 nA/cm^2, respectively, after polarizing them under an electric field of 3.0 kV/cm for 1 h at 400°C. Interestingly, in another work a commercially procured 75% porous HAp disk compact is shown to store a charge density of 13 $\mu C/cm^2$ where as a dense HAp block with a through hole (width $\sim$5 mm $\times$ breadth $\sim$5 mm $\times$ height $\sim$5 mm) exhibited a charge density of 2.6 $\mu C/cm^2$. Recently, influence of grain size and poling condition of HAp charge storage ability was investigated and experimentally shown that by increasing the HAp sintering temperature from 1250° to 1400°C, the stored charge density can be increased from 8.4 to 60 $\mu C/cm^2$ under identical poling condition ($T_p = 400$°C, $E_p = 5.0$ kV/cm, and $t_p = 1.0$ h) as the grain size of sintered HAp increased from 1.9 to 11 μm.

(3) In Vitro Bone Cell–Material Interactions

(A) Cell Morphology: In Fig. 4, poled and unpoled binary doped and undoped HAp samples surfaces are imaged after 7 days of culture to investigate bone cell attachment, growth and spreading on different surfaces. It can be observed that depending on the doping condition, surface charge and charge polarity of HAp samples, different levels of bioactivity on binary doped HAp (Figs. 4(a)–(c)) and undoped HAp (Figs. 4(d)–(f)) are possible. Overall, "N" poled surfaces of both binary doped HAp (Fig. 4(b)) and undoped HAp (Fig. 4(e)) samples demonstrate superior cell attachment and growth where osteoblasts cells form a well-flattened confluent layer covering the entire surface. In contrast, osteoblast adhesion has been found to be restricted on "P" poled sample surfaces where cells are mostly round in shape and less in number for both binary doped (Fig. 4(c)) and undoped HAp (Fig. 4(f)) samples. This observation is in good agreement with our previous *in vitro* cell culture results on pure polarized bulk and HAp-coated surfaces.[21,25] However and more importantly, binary dopant composition shows better cell–material interactions over undoped HAp samples when cells are seen to adhere to each other with cellular micro extensions and connected to the substrate in addition to the neighboring cells on "N" poled (Fig. 4(b)) and unpoled (Fig. 4(a)) binary-doped HAp surfaces as compared with unpoled and undoped HAp (Fig. 4(d)). Furthermore, better cell–material interactions on both binary doped "N" poled and unpoled can also evidenced from the presence of apatite granules as indicated by the arrows in the Figs. 4(a) and (b), respectively. These spherical granules of apatite deposition as observed on unpoled and "N" poled binary doped samples indicate the onset of biomineralization process.[21] Evidently, "N" poled surfaces of Sr^{2+}–Mg^{2+} binary doped HAp samples were found to have maximum bioactivity among all other surfaces with extensive flaky layers of cell proliferation and rough cellular surface suggesting multilayer proliferation of osteoblast cells.

(B) Cell Proliferation: The MTT assay study has been used to quantitatively determine the proliferation of viable hFOB cells on both poled and unpoled binary doped as well as undoped HAp samples. Figure 5 shows a comparison of optical densities illustrating hFOB cell proliferation on different samples after 3 and 7 days culture period. The advantage of dopant addition can be realized when improved bone cell viability and growth were observed on all binary doped HAp

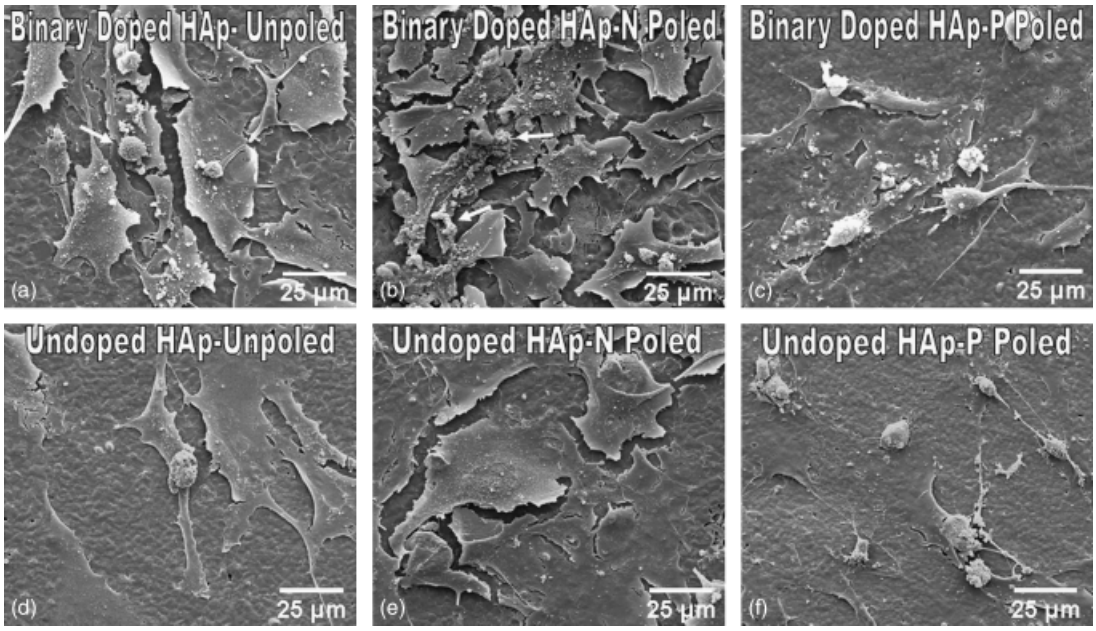

Fig. 4. SEM micrographs illustrating the hFOB cell adhesion and growth after 7 days of culture on poled and unpoled surfaces of (a–c) binary doped (1 wt% MgO+1 wt% SrO) HAp and (d–f) undoped HAp samples. "N", negatively charged surface, "P", positively charged surface, Arrows in the figures indicate the deposited apatite minerals.

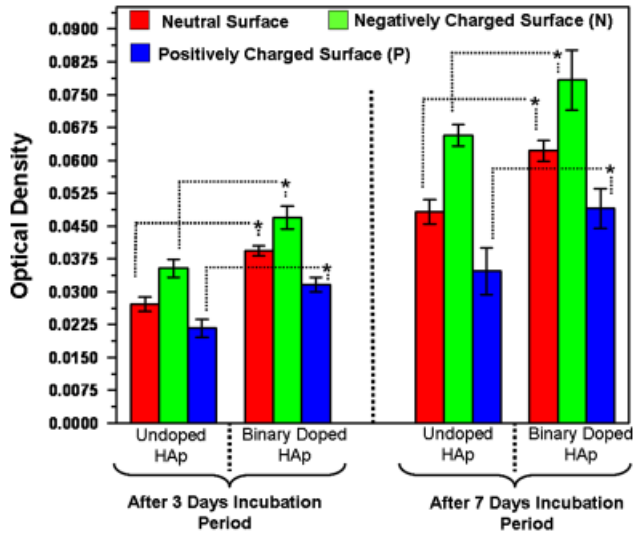

Fig. 5. MTT assay results illustrating hFOB cell proliferation on undoped HAp and binary-doped (1 wt% MgO+1 wt% SrO) HAp surfaces under poled as well as unpoled conditions after 3 and 7 days of culture time. Statistical analysis confirms that the differences in cell densities between undoped and binary doped samples are significant for all incubation periods ($^*P<0.05$).

samples in comparison with undoped HAp samples irrespective of poling condition as confirmed by the Student *t*-test ($P<0.05$) for both 3 and 7 days culture periods. Among polarized samples, the number of cells on the "N" poled HAp surfaces is always higher than that of unpoled HAp surface, while opposite growth kinetics can be observed for "P" poled surfaces where cell growth has been suppressed for all culture day periods. Evidently, the highest cell proliferation is observed on "N" poled HAp surfaces of binary doped HAp samples after 7 days. This superior biological properties can be explained by the higher surface charge storage of Sr^{2+}–Mg^{2+} ($\sim$4.19 $\mu C/cm^2$) binary doped samples, which is believed to accelerate the apatite mineralization and favored adsorption of cell adhesive proteins (e.g., integrins, fibronectin, vitronectin) for osteoblast cell adhesion on negatively charged surfaces.[18,21,25] Our results are in good agreement with previous investigations, which revealed that the presence of Mg^{2+} and Sr^{2+} can enhance osteoblast growth and favor the bone regeneration process by accelerating mineral metabolism and promoting catalytic reactions during bone remodeling process.[6–8,27] Our research findings clearly suggests that combined addition of MgO and SrO into polarized HAp ceramics as dopants can help us in developing a highly bioactive surface with tailored adhesion and adsorption properties that can potentially improve bone cell–material interaction toward faster bone tissue repairing and regeneration.

IV. Conclusions

In summary, our research on electro-thermally polarized doped HAp has experimentally showed that the addition of dopants has considerable influence on the HAp phase thermal stability and relative density, which in turn significantly controls the polarizability and charge storage ability of sintered HAp. It has been found that the combined addition of MgO–SrO dopants (binary dopants composition) in commercial HAp is most beneficial in enhancing the polarizability and charge storage ability by inhibiting the HAp phase decomposition. *In vitro* bone cell–material interaction study has been evidently showed that the presence of Mg^{2+} and Sr^{2+} can significantly improve osteoblast response and activities on negatively charged surface. The MTT assay results at 7 days clearly indicate the highest cell proliferation on negatively charged surfaces of binary doped HAp samples, while positively charged doped HAp surfaces exhibit limited cellular growth in comparison with neutral surfaces. Overall, our research results warrant further *in vivo* investigation to establish the potency of developing electrically polarized doped HAp ceramics as a viable biomaterial for clinical usage where we could gain several advantages of dopants accompanied with the original benefits of electrical polarization treatment.

References

[1]S. M. Best, A. E. Porter, E. S. Thian, and J. Huang, "Bioceramics: Past, Present and for the Future," *J. Eur. Ceram. Soc.*, **28**, 1319–27 (2008).
[2]L. L. Hench, "Bioceramics: From Concept to Clinic," *J. Am. Ceram. Soc.*, **74** [7] 1487–510 (1991).
[3]A. Bigi, G. Cojazzi, S. Panzavolta, A. Ripamonti, N. Roveri, M. Romanello, K. Noris Suarez, and L. Moro, "Chemical and Structural Characterization of the Mineral Phase from Cortical and Trabecular Bone," *J. Inorg. Biochem.*, **68** [1] 45–51 (1997).
[4]M. Driessens, V. Dijk, and M. Borg-greven, "Biological Calcium Phosphates and their Role in the Physiology of Bone and Dental Tissues I. Composition and Solubility of Calcium Phosphates," *Calcif. Tissue. Int.*, **26** [1] 127–37 (1978).
[5]A. Bandyopadhyay, S. Bernard, W. Xue, and S. Bose, "Calcium Phosphate Based Resorbable Ceramics: Influence of MgO, ZnO and SiO_2 Dopants," *J. Am. Ceram. Soc.*, **89** [9] 2675–88 (2006).
[6]C. Capuccini, P. Torricelli, F. Sima, E. Boanini, C. Ristoscu, B. Bracci, G. Socol, M. Fini, I. N. Mihailescu, and A. Bigi, "Strontium-Substituted Hydroxyapatite Coatings Synthesized by Pulsed-Laser Deposition: *In Vitro* Osteoblast and Osteoclast Response," *Acta Biomater.*, **4** [6] 1885–89 (2008).
[7]W. Xue, J. Moore, H. L. Hosick, S. Bose, A. Bandyopadhyay, W. W. Lu, K. Cheung, and K. Luk, "Osteoprecursor Cell Response to Strontium-Containing Hydroxyapatite Ceramics," *J. Biomed. Mater. Res. Part A*, **79A** [4] 804–14 (2006).
[8]T. J. Webster, E. L. Massa-Schlueter, J. L. Smith, and E. B. Slamovich, "Osteoblast Response to Hydroxyapatite Doped with Divalent and Trivalent Cations," *Biomaterials*, **25** [11] 2111–21 (2004).
[9]S. J. Kalita and H. A. Bhatt, "Nanocrystalline Hydroxyapatite Doped with Magnesium and Zinc: Synthesis and Characterization," *Mater. Sc. Eng. C*, **27** [4] 837–48 (2007).
[10]S. Kannan, J. H. G. Rocha, S. Agathopoulos, and J. M. F. Ferreira, "Fluorine-Substituted Hydroxyapatite Scaffolds Hydrothermally Grown from Aragonitic Cuttlefish Bones," *Acta Biomater.*, **3** [2] 243–49 (2007).
[11]S. Kannan, J. H. G. Rocha, and J. M. F. Ferreira, "Synthesis and Thermal Stability of Sodium, Magnesium Co-Substituted Hydroxyapatites," *J. Mater. Chem.*, **16** [3] 286–91 (2006).
[12]K. Yamashita and S. Nakamura, "Concept and Development of Vector Ceramics for Bio-Interface Engineering," *J. Ceram. Soc. Jpn.*, **113** [1] 1–9 (2005).
[13]F. R. Baxter, C. R. Bowen, I. G. Turner, and A. C. E. Dent, "Electrically Active Bioceramics: A Review of Interfacial Responses," *Ann. Biomed. Eng.*, **38** [6] 2079–2010 (2010).
[14]S. Nakamura, H. Takeda, and K. Yamashita, "Proton Transport Polarization and Depolarization of Hydroxyapatite Ceramics," *J. Appl. Phys.*, **10** [89] 5386–92 (2001).
[15]M. Ueshina, S. Nakamura, and K. Yamashita, "Millicoulomb Charge Storage in Ceramic Hydroxyapatite by Bimodal Electric Polarization," *Adv. Mater.*, **14** [8] 591–5 (2002).
[16]Y. Tanaka, T. Iwasaki, M. Nakamura, A. Nagai, K. Katayama, and K. Yamashita, "Polarization and Microstructural Consideration of Ceramic Hydroxyapatite Electrets," *J. Appl. Phys.*, **107** [1] 01407–10 (2010).
[17]K. Yamashita, N. Oikawa, and T. Umegaki, "Acceleration and Deceleration of Bone-Like Crystal Growth on Ceramic Hydroxyapatite by Electric Poling," *Chem. Mater.*, **8**, 2697–700 (1996).
[18]M. Ohgaki, T. Kizuki, M. Katsura, and K. Yamashita, "Manipulation of Selective Cell Adhesion and Growth by Surface Charges of Electrically Polarized Hydroxyapatite," *J. Biomed. Mater. Res. A*, **3** [57] 366–73 (2001).
[19]T. Kobayashi, S. Nakamura, and K Yamashita, "Enhanced Osteobonding by Negative Surface Charges of Electrically Polarized Hydroxyapatite," *J. Biomed. Mater. Res.*, **57**, 477–84 (2001).
[20]K. Iwasaki, Y. Tanaka, M. Nakamura, A. Nagai, K. Hashimoto, Y. Toda, K. Katayama, and K. Yamashita, "Rate of Bonelike Apatite Formation Accelerated on Polarized Porous Hydroxyapatite, Simulation of Bone Ingrowth on Polarized Porous Hydroxyapatite Ceramics," *J. Am. Ceram. Soc.*, **91** [12] 3943–9 (2008).
[21]S. Bodhak, S. Bose, and A. Bandyopadhyay, "Role of Surface Charge and Wettability on Early Stage Mineralization and Bone Cell–Materials Interactions of Polarized Hydroxyapatite," *Acta Biomater*, **5** [6] 2178–88 (2009).
[22]M. Nakamura, A. Nagai, T. Hentunen, J. Salonen, Y. Sekijima, T. Okura, K. Hashimoto, Y. Toda, H. Monma, and K. Yamashita, "Surface Electric Fields Increase Osteoblastic Adhesion through Improved Wettability on Hydroxyapatite Electret," *Appl. Mater. Interf.*, **1** [10] 2181–9 (2009).
[23]D. Kumar, J. P. Gittings, I. G. Turner, C. R. Bowen, A. Bastida-Hidalgo, and S. H. Cartmell, "Polarization of Hydroxyapatite: Influence on Osteoblast Cell Proliferation," *Acta Biomater.*, **6** [4] 1549–54 (2010).
[24]R. Kato, S. Nakamura, K. Katayama, and K. Yamashita, "Electrical Polarization of Plasma-Spray-Hydroxyapatite Coatings for Improvement of Osteoconduction of Implants," *J. Biomed. Mater. Res. A*, **74A** [4] 652–8 (2005).
[25]S. Bodhak, S. Bose, and A. Bandyopadhyay, "Electrically Polarized HAp-Coated Ti: *In vitro* Bone Cell–Material Interactions," *Acta Biomater.*, **6** [2] 641–51 (2010).
[26]W. Xue, H. L. Hosick, A. Bandyopadhyay, S. Bose, C. Ding, K. D. Luk, K. M. Cheung, and W. W. Lu, "Preparation and Cell–Materials Interactions of Plasma Sprayed Strontium-Containing Hydroxyapatite Coating," *Surf. Coat. Technol.*, **201** [8] 4685–93 (2007).

[27]S. S. Banerjee, S. Tarafder, N. M. Davies, A. Bandyopadhyay, and S. Bose, "Understanding the Influence of MgO and SrO Binary Doping on the Mechanical and Biological Properties of β-TCP Ceramics," *Acta Biomater.*, **6** [10] 4167–74 (2010).

[28]W. Xue, K. Dahlquist, A. Banerjee, A. Bandyopadhyay, and S. Bose, "Synthesis and Characterization of Tricalcium Phosphate with Zn and Mg Based Dopants," *J. Mater. Sc.: Mater. Med.*, **19**, 2669–77 (2008).

[29]A. Bandyopadhyay, E. A. Withey, J. Moore, and S. Bose, "Influence of ZnO Doping in Calcium Phosphate Ceramics," *Mater. Sc. Eng. C*, **27** [1] 14–7 (2007).

[30]Y. Yamasaki, Y. Yoshida, M. Okazaki, A. Shimazu, T. Uchida, T. Kubo, Y. Akagawa, Y. Hamada, J. Takahashi, and N. Matsura, "Synthesis of Functionally Graded $MgCO_3$ Apatite Accelerating Osteoblast Adhesion," *J. Biomed. Mater. Res.*, **62** [1] 99–105 (2002).

[31]S. G. Dahl, P. Allain, P. J. Marie, Y. Mauras, G. Boivin, P. Ammann, Y. Tsouderos, P. D. Delmas, and C. Christiansen, "Incorporation and Distribution of Strontium in Bone," *Bone*, **28**, 446–53 (2001).

[32]P. J. Marie, P. Ammann, G. Boivin, and C. Rey, "Mechanisms of Action and Therapeutic Potential of Strontium in Bone," *Calcif. Tissue. Int.*, **69**, 121–9 (2001).

[33]M. Yamaguchi, "Role of Zinc in Bone Formation and Bone Resorption," *J. Trace Elem. Exper. Med.*, **11** [2–3] 119–35 (1998).

[34]Z. P. Sun, B. Ercan, Z. Evis, and T. J. Webster, "Microstructural, Mechanical, and Osteocompatibility Properties of Mg(2+)/F(-)-Doped Nanophase Hydroxyapatite," *J. Biomed. Mater. Res. A*, **94A** [3] 806–15 (2010).

[35]R. Kumar, P. Cheang, and K. A. Khor, "RF Plasma Processing of Ultra-Fine Hydroxyapatite Powders," *J. Mater. Process. Technol.*, **113** [1–3] 456–62 (2001).

[36]C. Bucci, R. Fieschi, and G. Guidi, "Ionic Thermocurrents in Dielectrics," *Phys. Rev.*, **148** [2] 816–23 (1966).

[37]K. Yamashita, K. Kitagaki, and T. Umegaki, "Thermal Instability and Proton Conductivity of Ceramic Hydroxyapatite at High Temperatures," *J. Am. Ceram. Soc.*, **78**, 1191–7 (1995).

[38]A. J. Ruys, M. Wei, C. C. Sorrell, M. R. Dickson, A. Brandwood, and B. K. Milthorpe, "Sintering Effects on the Strength of Hydroxyapatite," *Biomaterials*, **16** [5] 409–15 (1995).

[39]C. K. Wang, C. P. Ju, and J. H. C. Lin, "Effect of Doped Bioactive Glass on Structure and Properties of Sintered Hydroxyapatite," *Mater. Chem. Phys.*, **53** [2] 138–49 (1998).

[40]A. Bigi, E. Foresti, M. Gandolfi, M. Gazzano, and N. Roveri, "Inhibiting Effect of Zinc on Hydroxylapatite Crystallization," *J. Inorg. Biochem.*, **58** [1] 49–58 (1995).

[41]M. A. Barbosa, F. J. Monteiro, R. Correia, and B. Leon, "Preparation and Properties of Zinc Containing Biphasic Calcium Phosphate Bioceramics," *Key Eng. Mater.*, **254–256**, 119–22 (2004).

[42]M. Li, X. Xiao, R. Liu, C. Chen, and L. Huang, "Structural Characterization of Zinc-Substituted Hydroxyapatite Prepared by Hydrothermal Method," *J. Mater. Sc.: Mater. Med.*, **19** [2] 797–803 (2008).

[43]S. Kannan, F. Goetz-Neunhoeffer, J. Neubauer, and J. M. F. Ferreira, "Synthesis and Structure Refinement of Zinc-Doped β-Tricalcium Phosphate Powders," *J. Am. Ceram. Soc.*, **92** [7] 1592–5 (2009).

[44]C. M. Mardziah, I. Sopyan, and S. Ramesh, "Strontium-Doped Hydroxyapatite Nanopowder via Sol–Gel Method: Effect of Strontium Concentration and Calcination Temperature on Phase Behavior," *Trends Biomater. Artif. Org*, **23** [2] 105–13 (2009). □